VOLUME 119, NUMBER 29
JULY 23, 1997

JOURNAL OF THE AMERICAN CHEMICAL SOCIETY

Nanosecond Molecular Dynamics Study of a Polycation Ribonucleic Guanidine (RNG) Duplexed with a Complementary DNA Oligomer Strand

Jia Luo and Thomas C. Bruice*

Contribution from the Department of Chemistry, University of California at Santa Barbara, Santa Barbara, California 96310

Received January 21, 1997[⊗]

Abstract: Replacement of the phosphodiester linkages of the polyanion RNA with guanidinium linkers provides the polycation ribonucleic guanidine (RNG). Molecular dynamics studies to 1080 ps of the hybrid duplex formed from an octameric RNG strand $r(Ag)_8$ with a complementary DNA oligomer strand $d(Tp)_8$ have been carried out with explicit water solvent and Na^+Cl^- counterions under periodic boundary conditions with use of the CHARMM force field and Ewald summation method. The Watson−Crick hydrogen bonding pattern of the A/T tracts was maintained intact through the simulation without any structural restraints. Even for the two ends, only one end was partially frayed. The overall structure is equilibrated at a B-DNA conformation, and the RNG strand takes on the general conformation of the DNA backbone. The structural history of the RNG·DNA duplex was determined by examining histograms from the dynamics run. The histograms are of the hydrogen bonding pattern (sequence recognition) and base pair opening occurrences, minor groove width narrowing (3 Å), and bending of tracts. The bending angle measured between the local axis vectors of the first and last helical axis segments is about 33° for the averaged structure. Propeller twist (associated with three-centered hydrogen bonding) up to −30°, native to DNA AT base pairing, was also observed. The sugar pseudorotation phase angles and the ring rotation angles for the DNA strand are within the C3′-endo domain. However, for the RNG strand the pseudorotation angles converted to O4′-endo.

Introduction

Replacement of the phosphodiester linkages of the polyanions RNA and DNA with guanidine linkers provides polycationic ribonucleic and deoxyribonucleic guanidine (RNG and DNG, respectively).[1−5] RNG and DNG are novel new materials with great promise in biological research and as sources of putative drugs. (Chart 1 shows the RNG oligomer of importance in the present investigation.) Oligonucleotide analogs capable of arresting cellular processes at the translational and transcriptional levels via specific sequence recognitions of RNA and DNA, respectively, are known as antisense and antigene agents.[6−10] Key goals in the design of such agents include the following: increased binding ability to nucleic acid receptors with fidelity

[⊗] Abstract published in *Advance ACS Abstracts,* July 1, 1997.

(1) Dempcy, R. O.; Almarsson, O.; Bruice, T. C. *Proc. Natl. Acad. Sci. USA* **1994**, *91*, 7864
(2) Dempcy, R. O.; Browne, K. A.; Bruice, T. C. *J. Am. Chem. Soc.* **1995**, *117*, 6140.
(3) Dempcy, R. O.; Browne, K. A.; Bruice, T. C. *Proc. Natl. Acad. Sci. USA* **1995**, *92*, 6097.
(4) Browne, K. A.; Dempcy, R. O.; Bruice, T. C. *Proc. Natl. Acad. Sci. USA* **1995**, *92*, 7051.
(5) (a) Dempcy, R. O.; Luo, J.; Bruice, T. C. *Proc. Natl. Acad. Sci. USA* **1996**, *93*, 4326; (b) Blaskó, A.; Dempcy, R. O.; Minyat, E. E.; Bruice, T. C. *J. Am. Chem. Soc.* **1996**, *118*, 7892.
(6) Uhlmann, E.; Peyman, A. *Chem. Rev.* **1990**, *90*, 543.
(7) Crooke, S. T. *Annu. Rev. Pharmacol. Toxicol.* **1992**, *32*, 329.
(8) Crooke, S. T. *FASEB J.* **1993**, *7*, 533.
(9) Cook, P. D. In *Antisense Research and Applications*; Crooke, S. T., Lebleu, B., Eds.; CRC: Boca Raton, FL, 1993; pp 149−187.
(10) Sanghvi, Y. S.; Cook, P. D. In *Nucleosides and Nucleotides as Antitumor and Antiviral Agents*; Chu, C. K., Baker, D. C., Eds.; Plenum: New York, 1993; pp 311−324.

S0002-7863(97)00188-1 CCC: $14.00

Chart 1

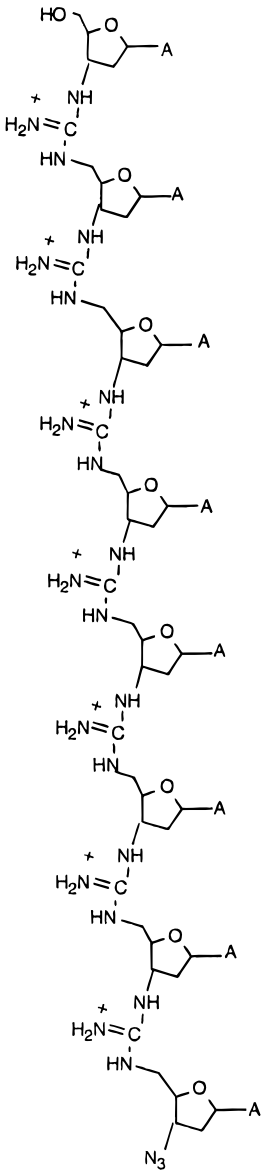

of sequence recognition, and resistance to the degradation by nucleases and increased membrane permeability. Replacement of the phosphodiester linkages by the guanido linker renders the resultant structures impervious to nuclease attack. This substitution leaves Watson−Crick base-pairing interactions intact and provides additional electrostatic attractions with targeted nucleic acid. The positive charge of the linker [−NH−C(=N^+H_2)−NH−] of DNG/RNG has an electrostatic attraction to the negative phosphodiester [−O−(PO_2^-)−O−] linker of DNA/RNA. Moreover, a RNG complex with a complementary strand of natural DNA/RNA will exhibit a net neutral charge, a feature which should facilitate cellular uptake. Our previous thermodynamic studies showed that a pentameric thymidyl DNG, $d(Tg)_4$-T-azido, is specific for its complementary tracts of poly(dA) but does not interact with polyguanylic, polycytidylic, or polyuridylic tracts. With the short sequences $d(Ap)_x$ ($x = 5$ to 13) the pentamer $d(Tg)_4$-T-azido forms triple-helical structures with T:A = 2:1, double strands being undetectable in favor of triplex structures.[5b] The thermodynamic stability of guanido nucleotide triple helices makes NMR and X-ray examination of structures of double strand DNG·DNA and RNG·DNA unlikely. Knowledge of the structure of DNG·DNA and RNG·DNA duplexes as the building blocks is, however, of importance in our understanding of triplex stabilities.

In this study we have used molecular dynamics simulations in water to investigate the dynamic conformations of $r(Ag)_8$-$d(T_p)_8$, a RNG·DNA hybrid duplex. We have focused on the hydrogen-bonding pattern, the stability and nature of the hybrid complexes, and especially the bending and the minor groove narrowing due to electrostatic attraction of RNG and the DNA. Theoretical simulations of DNA structure have a rich history, as discussed in reviews by Beveridge *et al.*[11a,b] Nanosecond molecular dynamics simulations with explicit solvent, counterions, and full periodic boundary conditions, as well as the Ewald method to overcome the long-range convergence problem, have been recently reported on triplex DNA (Weerasinghe *et al.*[12a]) and on duplex DNA without restraints (Cheatham *et al.*[12b]). The considerable agreement with the X-ray and NMR structures from the above two studies and the convergence of (two) different starting structures and (four) different trajectories leading to a consistent average structure in the latter study indicated that one can now begin to realistically examine sequence-dependent structural effects in DNA duplexes and triplexes using molecular dynamics. In this study, we have applied these molecular dynamics techniques to the RNG·DNA hybrid duplex eight base pairs in length.

Computational Experiments

Model building and computations were performed on a Silicon Graphics workstation with CHARMM[13a,b] version 22.5 release and Quanta version 4.0 (MSI, Waltham, MA, currently, Biosym/MSI, San Diego, CA). The RNG·DNA double helical hybrid [$r(Ag)_8$·$d(Tp)_8$] was built by using the method described in previous publications from this laboratory.[1,3,5] A Watson−Crick base-paired octomeric duplex of A-DNA [$d(Ap)_8$·$d(Tp)_8$] was made by using Nucleic Acid Builder in Quanta. The sugars of the purine strand were converted from deoxyriboses to riboses by replacing the H2′ protons with hydroxyl groups; guanidinium groups [−NH−C(=N^+H_2)−NH−] were overlapped on the phosphate linkages [−O−(PO_2^-)−O−] of the purine strand; sodium ions were placed adjacent to the phosphate moieties along the pyrimidine strand, and chloride ions were placed near the guanidinium groups. The solutes were placed in a cubic box of dimensions 35.10 × 34.18 × 33.59 Å with the helical axis parallel to the *z*-direction. Water molecules (1791) were placed in the box and those with close contacts to the solute atoms (within 2.6 Å) were excluded from the solution, leaving a total of 1467 water molecules in the periodic boxes.

The CHARMM residue topology file DNAH.RTF was used for the standard DNA residues and was modified to use for RNG residues.[1,5] All atom CHARMM force field parameters were used in the simulations. Water molecules were treated as TIP3P residues.[13c] The initial velocities were generated by a Maxwell−Boltzman distribution at a temperature of 300 K. Periodic conditions were applied in all three directions. An accurate representation of long-range electrostatic interactions in MD simulations is extremely important. This is

(11) (a) Beveridge, D. L.; Swaminathan, S.; Ravishanker, G.; Withka, J. M.; Srinivasan, J.; Prevost, C.; Louise-May, S.; Langley, D. R.; DiCapua, F. M.; Bolton, P. H. In *Water and Biological Molecules*; Westhof, E., Ed.; Macmillan Press: Riverside, NJ, 1993; pp 165−225. (b) Beveridge, D. L.; Ravishanker, G. *Curr. Opin. Struct. Biol*. **1994**, *4*, 246.

(12) (a) Weerasinghe, S.; Smith, P. E.; Mohan, V.; Cheng Y.-K.; Pettitt, B. M. *J. Am. Chem. Soc*. **1995**, *117*, 2147. (b) Cheatham, T. E., III; Kollman, P. A. *J. Mol. Biol*. **1996**, *259*, 434.

(13) (a) Brooks, B. R.; Bruccoleri, R. E.; Olafson, B. D.; States, D. J.; Swaminathan, S.; Karplus, M. *J. Comput. Chem*. **1983**, *4*, 187. (b) MacKerell, A. D., Jr.; Wiorkiewicz-Kuczera, J.; Karplus, M. *J. Am. Chem. Soc*. **1995**, *117*, 11946. (c) Jorgensen, W. L.; Chandrasekhar, J.; Madura, J. D. *J. Comput. Chem*. ***1983***, *14*, 89.

particularly true for highly charged systems, such as DNA and RNA.[14a−c] The Ewald summation method[14d] was used to overcome the electrical static potential convergence problem caused by the cutoff due to the excess amount of computation time required for the simulation method used. The assemblies were minimized prior to dynamics runs to remove the strain in the initial structures. One hundred steps of steepest descent algorithm minimization were followed by the Adopted Basis Newton−Raphson algorithm minimization for 5000 steps. Nonbonding interactions were cut off at 10 Å. Dynamics for the assembly to 1080 ps, using a step of 0.002 ps and the SHAKE bond constraints,[15] were run with Verlet integration. Hydrogen bonds were not restrained during the simulation since free MD (dynamics without restraints) is a more natural and ideal way of simulation.

The Ewald[14d,e] method derives the electrical static potential to be the sum of real space and reciprocal space contributions (eqs 1 and 2),

$$\Phi_{\text{real}}(\mathbf{r},\beta) = \sum_{n} \text{erfc}(\beta|\mathbf{r}+\mathbf{n}|)/|\mathbf{r}+\mathbf{n}| \quad (1)$$

$$\Phi_{\text{recip}}(\mathbf{r},\beta) = 1/\pi V \sum_{m\neq 0} \exp(-\pi^2\mathbf{m}^2/\beta^2)\exp(2\pi i\mathbf{m}\cdot\mathbf{r})/\mathbf{m}^2 \quad (2)$$

where erfc( ) is the complementary error function, V is the volume of the periodic box, and n and m are the real and reciprocal space indices. β is a positive parameter—the value of β adjusts the relative rates of convergence of the real and reciprocal space sums. A heating phase of 6 ps for a final temperature near 300 K was followed by an initial equilibrium of 234 ps and a second phase of equilibration of 400 ps, and finally 400 ps for observance. During the initial equilibration, the velocities were scaled to maintain a temperature near 300 K. Trajectory coordinates were saved every 0.2 ps, giving 2000 structures for analysis of the average structure from the last 400 ps of MD, which represents the equilibrated collection phase. However, in order to visualize the structural evolution history, the histograms for the hydrogen bonding and the bending feature include the second-phase equilibration; for the minor groove width the histogram covers the whole simulation time span, including the heating stage. For the equilibrium period the structures were saved less frequently.

Results and Discussions

Molecular dynamics runs were performed on the RNG·DNA double helical hybrid [r(Ag) $_8$·d(T$_p$)$_8$] in water under the periodic boundary conditions with use of the Ewald summation method for long-range interactions (Experimental Section). The molecular dynamics results and statistical analyses were extracted from the 1080-ps trajectory and are based on the 2000 sample structures during the last 400 ps of the dynamics run. Detailed results of the simulations and the structural properties of the hybrid duplex are presented in what follows.

Throughout the nanosecond dynamics simulation and without structural constraints the hybrid duplex structure with hydrogen bondings (Chart 2) remained intact. Even the two ends were not frayed. At one end two hydrogen bonds were kept in position and at the other end one of the hydrogen bonds was intact. We would find both ends unraveled with conventional DNA or RNA duplex oligomers. However, the helical parameters, with few exceptions, phase transferred[12d] to the neighborhood of a B-DNA frame. For example, the second base pair next to the 3′ end (T6-A11) showed a certain degree of unwinding, and at the base pair second to the 5′ end (T3-A14 base step) there is a change in the rise.

It is interesting to note that at the second base pair next to both 5′ or 3′ ends, the base steps undergo certain degrees of either unwinding or change of rise. We will discuss this aspect later. Most backbone torsional parameters remained unchanged from the conventional A-DNA/RNA backbone values. With time certain RNG strand backbone torsion angles, which describe the geometries around the guanidinium group, change from the initially assumed standard A-RNA values. This relaxation relieves the tensions due to the replacement of the phosphate by guanidinium groups. And more importantly, after equilibration a new helical geometry was established, as well as base pair hydrogen bonding, which marks the sequence recognition specificity.

Chart 2

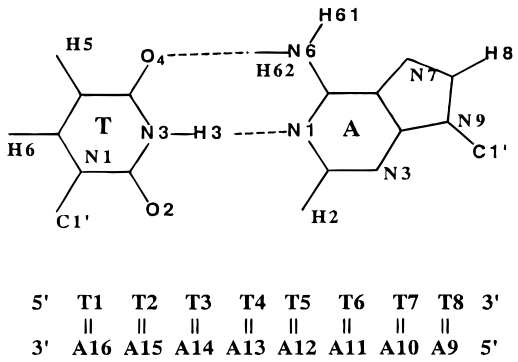

Counterions have diffused away from their counter partners during the 1080-ps run as far as 36 Å. The counterions near two ends are most remote. All Na^+ ions are more than 6.5 Å away from their original counter phosphate-P's. Cl^- ions are moving slower, more than 4.5 Å away from their original counter guanidinium-C's, because the atomic mass of Cl^- is higher than that of Na^+, except the counterions at A4 and A6 remain within *ca.* 3 Å of the starting positions. Due to the internal cancellation of overall charge, Na^+ and Cl^- are more prone to drift away from an RNG·DNA pair than Na^+ from a RNA·DNA pair.

Base Pair Hydrogen Bonding Pattern. To visualize the representative hydrogen bonding pattern (as shown in Chart 2), the histograms of Figure 1 may be examined. Figure 1a shows the hydrogen bond distances of H3−N1 and O4−H62 for the central bases T4-A13 and T5-A12, respectively. Figure 1b shows the heavy atom distances involved with the relevant hydrogen bondings provided in Figure 1a. Note that these distance histograms exhibit concerted openings and breathings between base pairs for both hydrogen bondings and heavy atom distances. The base openings are more pronounced in the major groove side (O4−H62). One should also note that the two hydrogen bondings within the same base pair have complementary motions. After equilibration, the observed base-opening periods measure around 100 ps, much as found by Weerasinghe *et al.*[12a] in studies with DNA. From the 5′ end to the 3′ end, the AT base pair hydrogen bondings are well maintained during the nanosecond dynamics run without restraining. An exception is seen in the hydrogen bonding at the 5′ end base pair H3−N1, which is flanked away. It is interesting to note that at the 5′ and 3′ ends the heavy atoms O4 and N6 are hydrogen bonded through H61−O4 rather than H62−O4 as observed in the central base pairs. The hydrogen-bonding pattern for the end base pairs T1-A16 (O4−H61) and T8-A9 (O4−H61, H3−N1) (Figure 2a for hydrogen bonding distances and Figure 2b for heavy atom distances, respectively) represents well-maintained Watson−Crick base pairing. These base pairings are probably further stabilized by the mutual attraction of the poly cation and polyanion backbones.

Three-centered bifurcated (propellar twist) hydrogen bond-

(14) (a) York, D. M.; Darden, T. A.; Petersen, L. G. *J. Chem. Phys.* **1993**, *99*, 8345. (b) Schreiber, H.; Steinhauser, O. *Biochemistry* **1992**, *31*, 5856. (c) Steinbach, P. J.; Brooks, B. R. *J. Comput. Chem.* **1994**, *15*, 667. (d) De Leeuw, S. W.; Perram, J. W.; Smith, E. R. *Proc. R. Soc. London, Ser. A* **1980**, *373*, 27.

(15) Van Gunsteren, W. F.; Berendsen, H. J. C. *Mol. Phys.* **1977**, *34*, 1311.

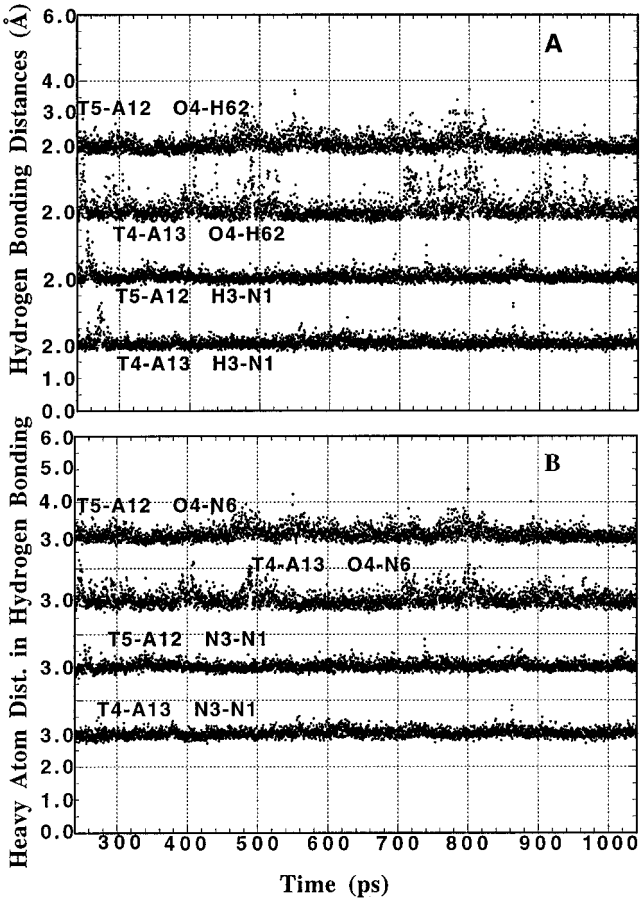

Figure 1. (A) The hydrogen bonding (H3−N1) and (O4−H62) distance dynamics histograms for the central base pairs T4-A5 and T5-A4 from 240 to 1040 ps. (B) The distance histogram between the heavy atoms (N3−N1) and (O4−N6) involved in the hydrogen bonding.

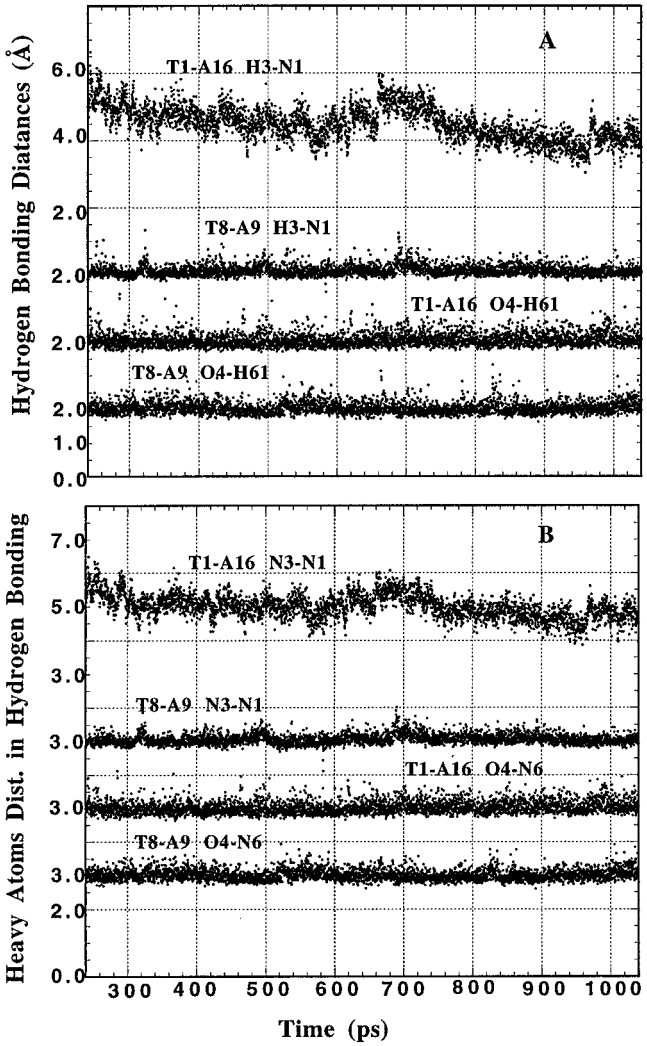

Figure 2. (A) The hydrogen bonding (H3−N1) and (O4−H61) distance dynamics histograms for 5′ end base pair T1-A8 and 3′ end base pair T8-A1 from 240 to 1040 ps. (B) The distance histogram between the heavy atoms (N3−N1) and (O4−N6) involved in the hydrogen bonding.

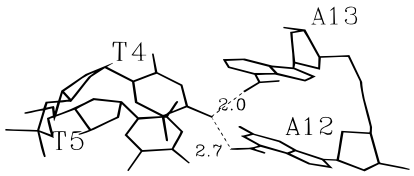

Figure 3. A snapshot of T4T5 and A12A13 base pairing and their bifurcating hydrogen bondings: H3(4)−N1(13), O4(4)−H62(13), and O4(4)−H62(12)—the bifurcating one.

ings[16] are often observed for AT tracts. The high degree of propeller twist helps maximize purine−purine stacking interactions and creats a potential system of additional hydrogen bonds. The extra hydrogen bond will certainly be of greater significance in the stablization of base pairing between the two strands. On the other hand, the three-centered bifurcated bondings often contribute to the bending of the tract.[16] In our 1080-ps dynamics trajectory, three-centered hydrogen bonding was also observed. A snapshot of T4T5 and A12A13 base pairing and their bifurcating is shown in Figure 3. The bifurcating bond distances with time are presented in Figure 4 for O4−H62 of T2-A14, T3-A13, T4-A12, and T6-A10. The hydrogen bond distances are less than 2.5 Å in 10% to 80% of the time span as shown in the figures. The propeller twists associated with these bifurcations are considered when describing the helical parameters *(vide intra)*.

The Minor Groove Width and Hydration. In Figure 5 we present the histogram of the minor groove width during the 1-ns dynamics run. The minor groove widths are measured from the phosphate-P of the T tract to the closest guanidinium-C of the A tract. Figure 5 is the histogram of the minor groove width measured from the phosphate-P of T6 to the guanidinium-C of A14. The histogram shows that attainment of equilibration at the minor groove width took at least about 500 ps. After equilibration (Figure 5) the average minor groove width is about 8.3 Å,[17c] which is 3 Å shorter than the crystal B-DNA minor groove width.[17a,b] Table 1 records the overall minor groove width (phosphate-P to guanidinium-C distances) of the average structure over the dynamics run. The results were obtained with use of the NEWHELIX 93 program.[17d] In the distance matrix, the DNA strand runs 5′ to 3′ down from top to bottom with the column representing T2 → T8, whereas the RNG strand runs

(16) (a) Nelson, H. C. M.; Finch, J. T.; Luisi, B. F.; Klug, A. *Nature* **1987**, *330*, 221. (b) Coll, M.; Frederick, C. A. Wang, H.-J.; Rich, A. *Proc. Natl. Acad. Sci. U.S.A.* **1987**, *84*, 8385.

(17) (a) Conner, B. N.; Takano, T.; Tanaka, S.; Itakura, K.; Dickerson, R. E. *Nature* **1982**, *295*, 294. (b) Dickerson, R. E. *Sci. Am.* **1983**, *249* (6), 94. (c) Minor groove width was defined[17a,b] as the centered atom distance less the van de Waals radius; van de Waals radius is taken as 5.8 Å[17a,b] for the two centered atoms, phosphate-P and guanidinium-C. (d) Prive, G. G.; Yanagi, K.; Dickerson, R. E. *J. Mol. Biol.* **1991**, *217*, 177.

(18) (a) Liepinsh, E.; Otting, G.; Wuthrich, K. *Nucleic Acids Res.* **1992**, *25* (24) 6549. (b) Otting, G.; Liepinsh, E. *Acc. Chem. Res.* **1995**, *28*, 171. (c) Sigler, P. B. *Proceedings of the Robert A. Welch Foundation 37th Conference on Chemical research*; Robert A. Welch Foundation: Houston, 1993; Chapter 5.

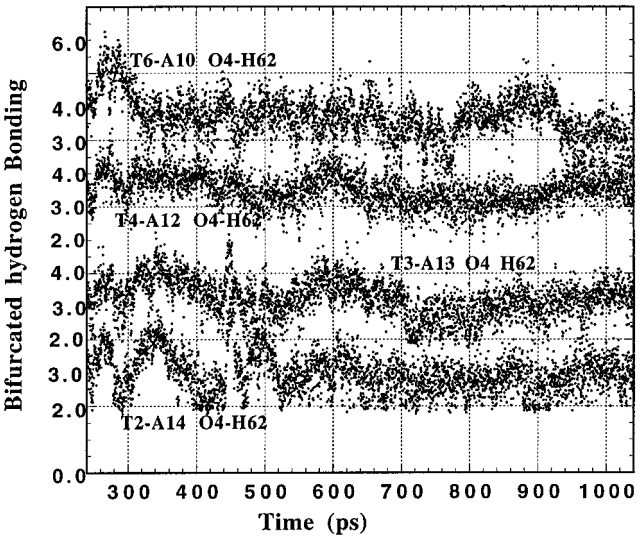

Figure 4. Three-centered bifurcating hydrogen bonding (O4−H62) distance histograms for T2-A14, T3-A13, T4-A12, and T6-A10 from 240 to 1040 ps.

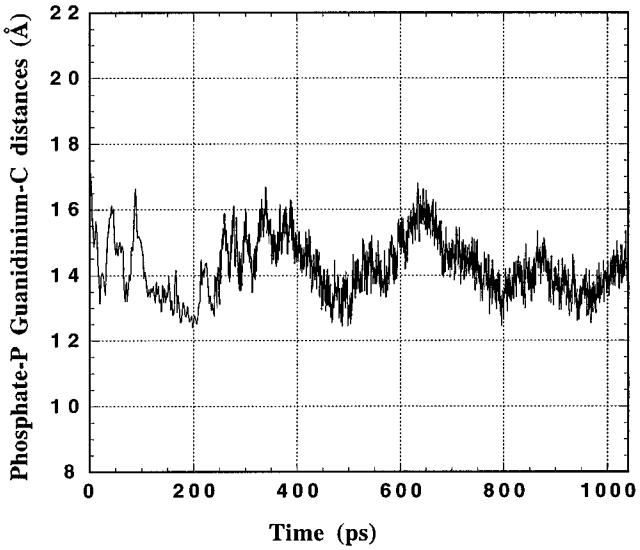

Figure 5. Minor groove width (phosphate-P to guanidinium-C distance) histogram from 40 to 1040 ps measured from T6 to A14 across the minor groove.

5′ to 3′ across from left to right with the horizontal line representing A10 → A16. By examining the matrix minor groove widths (Table 1), the shortest phosphate-P to guanidinium-C distances across the minor groove are 6.9, 7.7, 8.3, 8.4, and 7.4 for T4-A16, T5-A15, T6-A14, T7-A13, and T8-A12, respectively. It is apparent that the minor groove contraction is the result of polyanion and polycation backbone attractions. The fluctuations in the minor groove widths as shown in Figure 5 may well allow minor groove binders, such as the drug distamycin, to enter the minor groove. The width of the major groove does not vary by more than 1 Å from the crystal B-DNA major groove width.[17a,b]

Spines of hydration for both minor and major grooves are observed in the snapshots. Water molecules are hydrogen bonded in the major groove with thymine O4 and the adenine amino group, and in the minor groove with adenine H2 and thymine O2. The water molecules are constantly in fast exchange. The residence time of the water molecules at their hydration sites has been reported at the 0.1−1 ns time region by NMR experiments[18a,b] for DNA oligomers d(CGCGAATTCGCG)$_2$ and d(AAAAATTTTT)$_2$. In an averaged structure only those water molecules with longer residence time than the time span averaged over will remain in the hydration sites. In the average structure from our simulation two water molecules remain hydrogen bonded in the minor groove between T4 and T5, and T6 and T7 respectively, in a zigzag fashion.[17a] In the major groove at the positions of T2A15 and T3A14 base pairs, two hydrogen bonded water molecules remain throughout the last 400 ps with the second layer of water molecules observed in both positions. Thus a portion of the water spines in minor and major grooves have lifetimes equal to or longer than 0.4 ns. Structural water molecules mediating protein DNA interactions have been observed in the major groove[18c] by crystallographic studies.

Sugar Puckering. The sugar pseudorotation parameters,[19] obtained by use of NEWHELIX 93, are summarized in Table 2. The pseudorotation phase angles for the DNA strand, ranging from 8° to 42°, and the ring rotation angle ν' values for the strand are within the C3′-endo domain. Except for base T8 the pseudorotation phase angle and the ring rotation angle are off from the C3′-endo domain due to the end deformation effects. However, for the RNG strand the replacement of phosphate linkages by guanidinium linkages results in pseudorotation phase angle convertion to the O4′-endo domain, ranging from 83° to 118°. The ring rotation angles and δ backbone torsion angle for the RNG strand change accordingly. The pseudorotation phase angle (as ϕ) and δ torsion angle are also presented in the windows diagram for the backbone torsional angles in Figure 8, parts A and B. The results generated by the two programs NEWHELIX 93 and Curves, Dials and Windows are consistent with each other.

Helical, Axis, and Base Pair Parameters. In flexible systems like nucleic acids, an apparent conservation of structure over time may be the result of compensatory conformational changes in the systems. The helical axis and base pair parameters of the average structure (Figure 6) over the last 400-ps dynamics run are analyzed and extracted with the Curves, Windows-and-Dials programs,[20] so that the overall conformational variations along both strands for all the bases and base pairs can be perceived at a glance. The helicoidal description of a nucleic acid involves a set of 20 parameters.[21] The 20 parameters are divided into four groups: axis−base pair, axis, intra-base pair, and inter-base pair. The helicoidal parameters referenced to successive nucleotide base pairs are laid out in the graphics as "windows". In window's presentation, the horizontal axis represents the value of the parameter, and the vertical axis represents the possible time evolution for the dynamics histogram. The axis−base pair parameter variations along the helix are shown in Figure 7A, using window's single structure presentation for our averaged structure. X-displacement (XDP, Chart 3) and Y-displacement (YDP, Chart 3)

(19) (a) Saenger, W. *Principles of Nucleic Acid Structure*; Springer Verlag: New York, 1983. (b) McCammon, J. A.; Harvey, S. C. *Dynamics of Proteins and Nucleic Acids*; Cambridge University: Cambridge and New York, 1988. (c) Harvey, C. H.; Prabhakaran, M. *J. Am. Chem. Soc*. **1986**, *108* (20), 6128.

(20) (a) Ravishanker, G.; Swaminathan, S.; Beveridge, D. L.; Lavery, R.; Sklenar, H. *J. Biomol. Str. Dyn*. **1989**, *6*, 669. (b) Ramstein, J.; Lavery, R. *Proc. Natl. Acad. Sci. U.S.A.* **1988**, *85*, 7231.

(21) (a) Sarma, R. H. *J. Biomol. Struct. Dyn.* **1988**, *6* (3), 391. (b) Lavery, R.; Sklenar, H. *J. Biomol. Struct. Dyn.* **1989**, *6* (4), 655.

(22) Arnott, S.; Hukins, D. W. L. *Biochem. Biophys. Res. Comm*. **1972**, *47*, 1504.

(23) Arnott, S.; Hukins, D. W. L. *J. Mol. Biol*. **1973**, *81*, 93.

(24) Arnott, S.; Chandrasekaran, R.; Birdsall, D. L.; Leslie, A. G. W.; Ratliffe, R. L. *Nature* **1980**, *283*, 743.

(25) Fratini, A. V.; Kopka, M. L.; Drew, H. R.; Dickerson, R. E. *J. Biol. Chem*. **1989**, *257*, 14686.

(26) Dickerson, R. E.; Kopka, M. L.; Drew, H. R. In *Structure & Dynamics: Nucleic Acids and Proteins*; Clementi, E., Sarma, R. H., Eds.; Adenine Press: New York, 1983; pp 149−179.

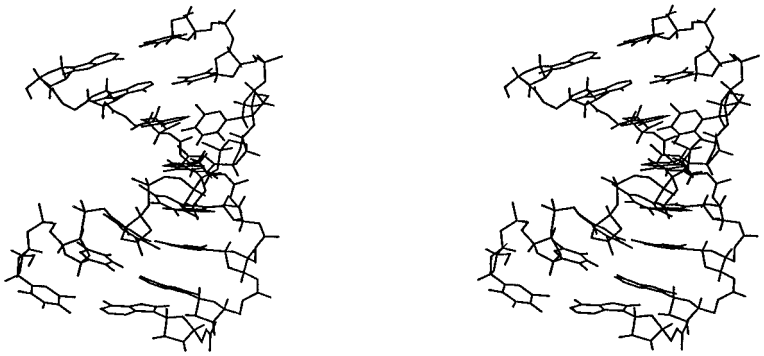

Figure 6. Average structure from the last 400 ps of the 1-ns dynamics run. The minor groove is shown in the lower portion.

Table 1. Phosphate-P−Guanidinium-C Distance Matrix (Å)

	A10	A11	A12	A13	A14	A15	A16
T2	12.0	12.9	14.3	15.7	15.8	14.7	12.2
T3	13.8	14.1	14.2	14.4	13.4	11.6	8.7
T4	16.1	15.7	14.5	13.5	11.4	9.2	6.9
T5	17.3	15.9	13.5	11.6	9.1	7.7	7.5
T6	16.9	14.9	11.9	9.8	8.3	9.1	11.1
T7	13.6	11.5	8.9	8.4	9.4	12.3	15.4
T8	11.6	9.3	7.4	8.7	12.0	16.4	20.2

Table 2. Sugar Pseudorotation Phase Angles

ν_0	ν_1	ν_2	ν_3	ν_4	pseudorotation	δ
			DNA Strand			
3.6	−27.0	38.0	−36.9	21.3	13.3	84.6
6.2	−24.9	32.9	−30.1	15.2	7.9	89.0
−5.3	−20.3	36.2	−39.8	28.7	25.7	79.3
−6.2	−19.6	35.8	−40.1	29.4	26.9	79.0
−7.4	−19.5	37.0	−41.9	31.1	28.1	77.2
−10.5	−14.8	32.2	−38.9	31.4	33.7	80.3
−15.9	−9.3	28.6	−38.4	34.3	42.0	81.3
−32.0	10.2	12.4	−30.9	39.8	71.3	86.6
			RNG Strand			
−40.5	21.3	3.4	−26.9	42.8	85.5	91.6
−40.3	20.3	4.5	−27.8	43.3	84.0	90.2
−41.9	21.3	4.4	−28.5	44.6	84.3	91.7
−41.2	22.0	2.6	−26.3	43.0	86.6	91.4
−42.3	20.6	6.0	−30.3	46.1	82.5	89.0
−41.2	21.0	4.2	−27.9	43.9	84.5	92.0
−45.1	34.4	−13.2	−12.3	36.3	107.6	109.8
−38.6	33.7	−17.9	−3.9	27.1	118.1	131.8
−24.9	4.3	15.4	−30.1	34.9	61.4	av
18.9	22.5	18.8	10.2	9.15	35.2	SD

specify the displacement of a nucleotide base pair from the helical axis, with X pointing into major groove of the duplex and the Y axis passing through purine C8 and pyrimidine C6. The parameters inclination (INC, Chart 3) and tip (TIP, Chart 3) are both positive for right-hand rotation. We refer the reader to the references for detailed definitions of all 20 parameters.[21] At this time we will only emphasize those that are more influential to the overall structural features. Both INC and TIP are diagnostic for A or B DNA/RNA. The templates at the bottom of Figure 7A for each column show the relevant reference values for standard A and B helical duplexes. For the RNG·DNA dimers of this study the INC parameter is generally that of a B conformation. However, TIP varies considerably away from 0 (which is standard for both A and B conformations) to negative angles. The variations in TIP are probably due to (1) the substitution of the backbone linker and (2) the irregularities, which also were observed earlier for the d(CGCGAATTCGCG)[22−26] DNA dodecamer.

The axis parameters, axis−X-displacement (AXD), axis−Y-displacement (AYD), axis inclination (AIN), and axis tip (ATP) for the average structure, are shown in Figure 7B. ATP (axis tip, Chart 4) is measured with respect to an overall helix axis for the duplex. The main deviations show up in ATP at the hinge points at junction steps T3-A14, T4-A13, T5-A12, and T6-A11, where the axis hinge changes direction at the center of the tract T5-A12. The total angle measured between the local axis vectors of the first and last helical axis segments is about 33°. In Figure 7C, the intra-base pair parameters are shown. More noticeable parameters are the propeller twist (PRP, the relative rotation between the two bases that are paired, Chart 4) and their openings (OPN, Chart 4). PRP up to −30° is native[20] to the DNA AT base pair. The AT propeller twist is pronounced because two hydrogen bondings per base pair is less stable than three hydrogen bondings per base pair as in GC pairing. In the propeller twist, a third hydrogen bond is obtained from the adjacent base pair as shown in Figure 3. The three-centered hydrogen bonding propeller twist (Figure 3) helps to stabilize the hybrid double helix. The base pair opening parameter (OPN), with the negative value indicative of an opening toward the minor groove, fluctuates less in the central tracts as compared to the ends. In addition it is found by an energy study[20b] that the opening process in DNA is greatly facilitated by bending, and once a base pair is disrupted by opening DNA can bend very easily.

The inter-base pair parameters are depicted in Figure 7D. Inspection of Figure 7D shows the positive sense ROL (roll, Chart 3) parameter ranges from 15° to 28°. The RIS parameter (vertical rise of helical bases, Chart 4) is kept at around 3.5 Å, which is typical for a B helix, with the exception at step 3, where the RIS is 2.2 Å. The TWS (helical twist angle per base pair, Chart 4) ranges from 30° to 40° with an exception at step 6, where the TWS is found as an unwinding value of 15°. Interestingly, both the unwinding and increased rise help to make room for bending since they provide more space in three dimensions.

Backbone Torsional Angles. Backbone torsional angles (Chart 5) were extracted from the average structures over the nanosecond dynamics trajectories. With the Windows-and-Dials program,[20] the conformational dials describing the numerical values of the torsional angles are obtained and presented in parts A and B of Figure 8 for DNA strand and RNG strand, respectively. The overall differences in the two strands are obvious. We use the terms gauche and trans to refer to broad regions of torsion angle space, and use Klyne−Prelog notation (synclinal, anticlinal, etc.)[19a] (Chart 6, IUPAC nomenclature for backbone torsion angles and the glycosidic tortions) when more specific designations are called for. The polyanion and polycation attractions caused changes relative to regular DNA/RNA backbones, mainly in the RNG strand around guanidine groups in torsional angles ζ (from −gauche to cis), α (from −gauche to trans), β (from trans to +gauche), and γ (to 90°, +gauche). The DNA strands were perturbed at the ϵ (from trans to

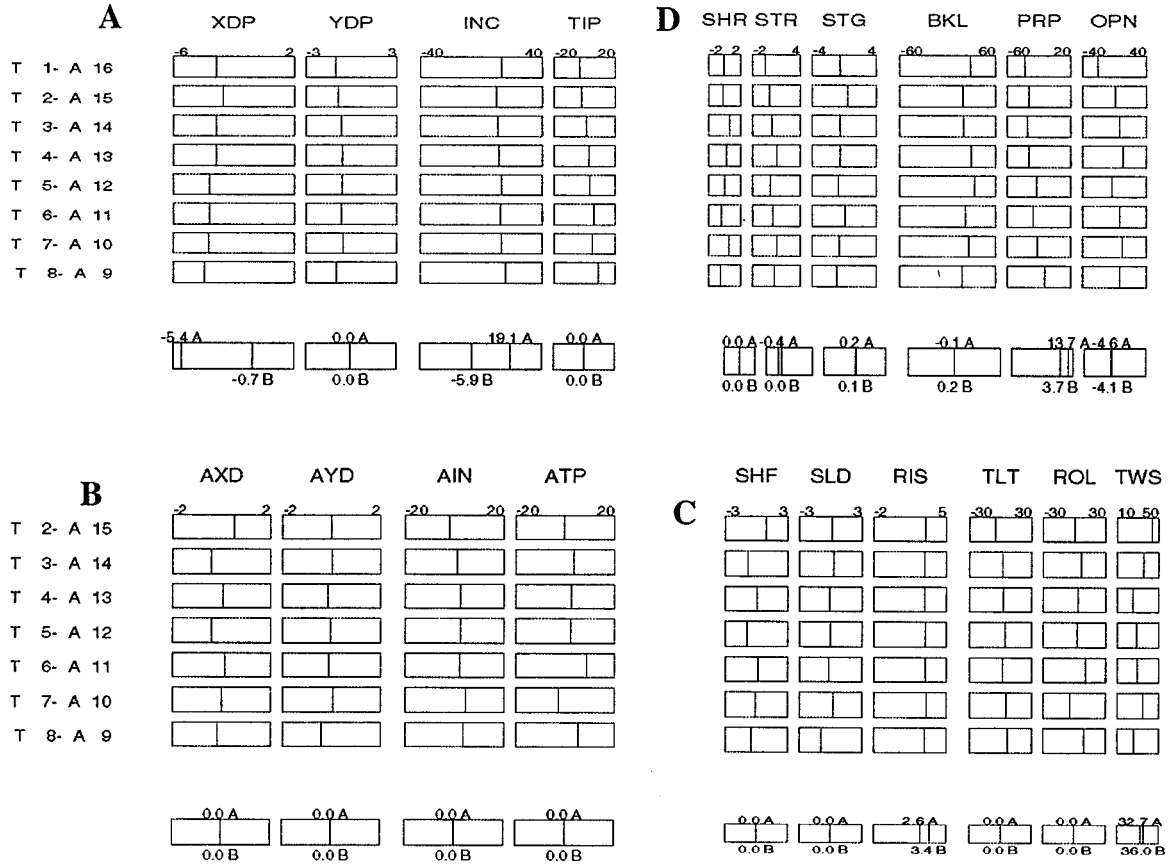

Figure 7. (A) Axis−base pair parameters for the average structure in window's single structure presentation—the horizontal axis represents the value of the parameter. X-displacement (XDP, the definition of XDP is depicted in Chart 3) and Y-displacement (YDP, the definition of YDP is depicted in Chart 3) specify the displacement of a nucleotide base pair from the helical axis X and Y, respectively, with X pointing into the major groove of the duplex and *Y* axis passing through purine C8 and pyrimidine C6. The parameters inclination (INC) is depicted in Chart 6 and tip (TIP) is depicted in Chart 3. The templates at the bottom of the figure for each column show the relevant reference value for the standard A and B helical duplex. (B) Axis parameters: axis−X displacement (AXD), axis−Y displacement (AYD), axis inclination (AIN), and axis tip (ATP) for the average structure. ATP (axis tip, the definition of ATP is depicted in Chart 4) is measured with respect to an overall helix axis for the duplex. The templates at the bottom of the figure for each column show the relevant reference value for the standard A and B helical duplex. (C) Six intrabase parameters for the average structure. More noticeable parameters are the propeller twist (PRP, the relative rotation between the two bases that are paired, as depicted in Chart 4) and the openings (OPN, Chart 4). PRP is native[20] to the AT base pair up to −30°. The negative value base pair opening parameter (OPN) is indicative of an opening toward the minor groove. The templates at the bottom of the figure for each column show the relevant reference value for the standard A and B helical duplex. (D) Six interbase pair parameters for the average structure. The positive sense ROL (roll, the definition of ROL is depicted in Chart 3) parameter ranges from 15° to 28°. The RIS parameter (vertical rise of helical bases, Chart 4) is kept at around 3.5 Å, which is typical for a B helix, with the exception at step 3, where the RIS is 2.2 Å. The TWS (helical twist angle per base, Chart 4) is ranging from 30° to 40° with the exception at step 6, giving an unwinding value of 15°. The templates at the bottom of the figure for each column show the relevant reference value for the standard A and B helical duplex.

Chart 3

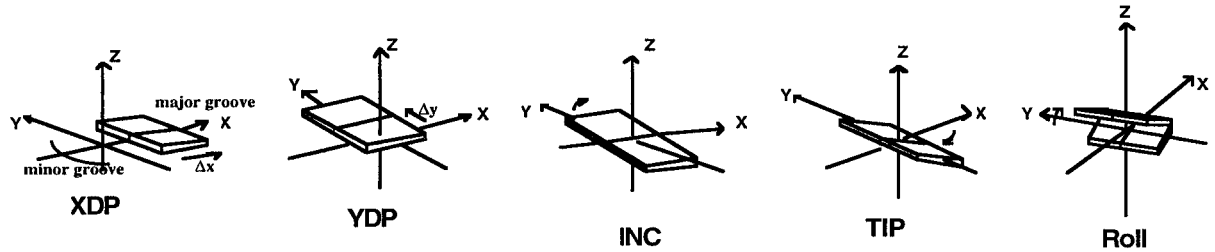

-anticlinal) and ζ (from -gauche to -anticlinal) to accommodate the attraction-caused deformation, but α and γ angles were only changed by one of the eight bases. Only β angles undergo similar changes for both RNG and DNA strands.

Is Bending Accompanyed by Strong Bifurcating? The bending features of DNA are important in transcription, replication, recombination, and other processes.[27−39] In Figure 9a,b we present the end-to-end distance histories of the DNA and RNG strands. Examination of these figures shows that both

(27) Liberles, D. A.; Dervan, P. B. *Proc. Natl. Acad. Sci. U.S.A.* **1996**, *93*, 9510.
(28) Thompson, J. F.; Landy, A. *Nucleic Acids Res.* **1988**, *16*, 9687.
(29) Goodman, S. D.; Nicholson, S. C.; Nash, H. A. *Proc. Natl. Acad. Sci. U.S.A.* **1992**, *89*, 11910.
(30) Hallet, B.; Rezsohazy, R.; Mahillon, J.; Delcour, J. *Mol. Microbiol.* **1994**, *14*, 131.
(31) Goryshin, I. Y.; Kil, Y. V.; Reznikoff, W. S. *Proc. Natl. Acad. Sci. U.S.A.* **1994**, *91*, 10834.
(32) Henriquez, V.; Milisavljevic, V.; Kahn, J. D.; Gennaro, M. L. *Gene* **1993**, *134*, 93.

Chart 4

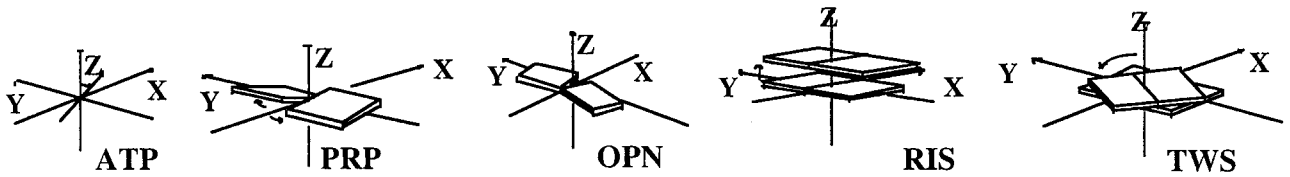

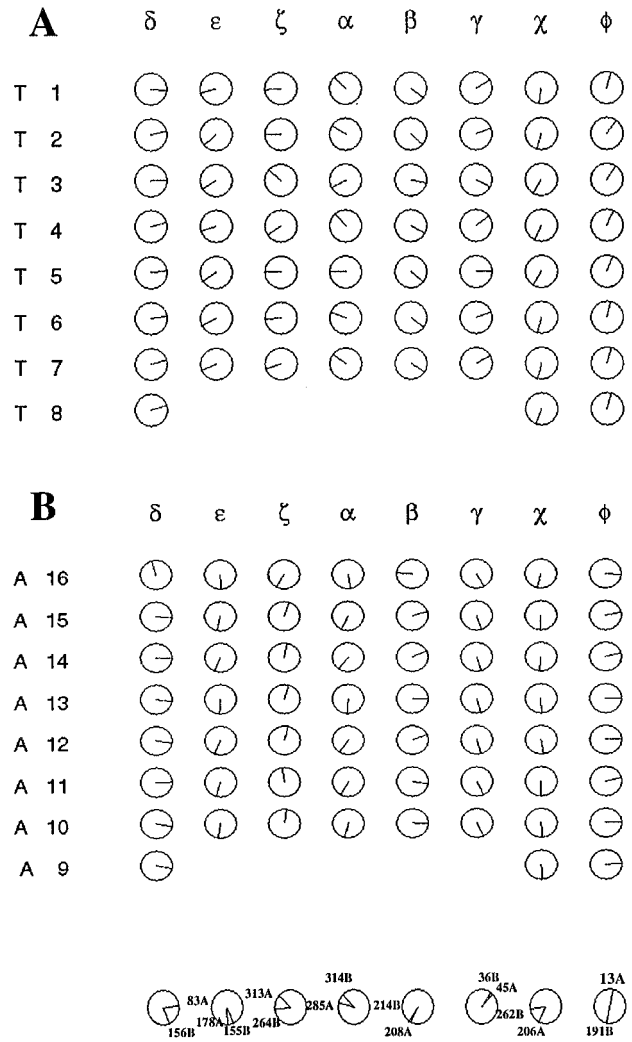

Figure 8. Backbone torsional conformations for the average structure in the dials single structure presentation—the radius points to the value of the torsional angles for the T (A) and A (B) strands. See Charts 5 and 6 for the definitions of the torsional parameters and the geometrical ranges. The templates at the bottom of the figure for each column show the relevant reference value for the standard A and B helical duplex.

ends are moving at the same pace, which shows DNA and RNG strands are well correlated after the duplex is equilibrated. The variations in the end-to-end length certainly reflect the helical bending.

Chart 5

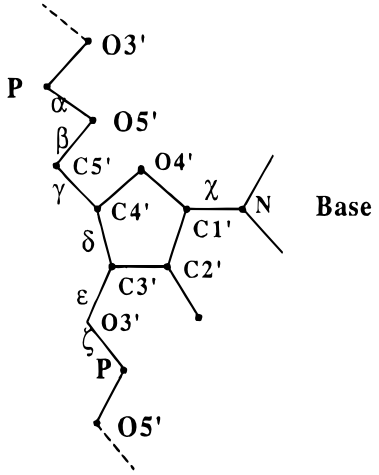

Chart 6

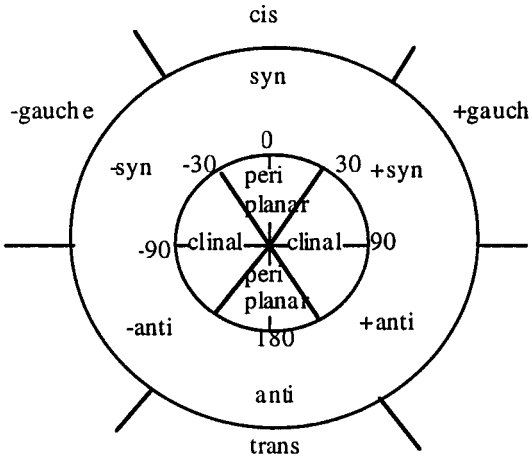

Strauss *et al.*[40] synthesized DNA duplexes in which cytosine bases are modified at the 5 position by the addition of an amino group, tethered by a hexamethylene chain. They showed that tethering six ammonium ions on one helical face causes DNA to bend by about 5°. From the helical parameter analyses in our study, using the average structure, we conclude that bending is induced upon substitution of guanidine [−NH−C(=N^+H_2)−NH−] for phosphate linkages. The bending is obvious on examination of the roll coordinate in Figure 7d, which showes a significant macroscopic curvature of structure. The total angle measured between the local axis vectors of the first and last helical axis segments is about 33°. Thus we may conclude that complexing of our RNG to its complementary DNA enhances the bending capability of the DNA. Our results lend credence to the hypothesis, that DNA-binding proteins change the shape of DNA by asymmetric neutralization of phosphate charges.[27−39]

Conclusions

We have performed 1080 ps molecular dynamics simulation on the hybrid RNG·DNA duplex $r(Ag)_8$·$d(Tp)_8$ in water with

(33) Nakajima, M.; Sheikh, Q. I.; Yamaoka, K.; Yui, Y.; Kajiwara, S.; Shishido, K. *Mol. Gen. Genet.* **1993**, *237*, 1.
(34) Muller, H. P.; Varmus, H. E. *EMBO J.* **1994**, *13*, 4704.
(35) Milot, E.; Belmaaza, A.; Rassart, E.; Chartrand, P. *Virlogy* **1994**, *201*, 408.
(36) Natesan, S.; Gilman, M. Z. *Genes Dev.* **1993**, *7*, 2497.
(37) Meacock, S.; Pescini-Gobert, R.; DeLamarter, J. F.; van Huijsduijen, R. H. *J. Biol. Chem.* **1994**, *269*, 31756.
(38) Kim, J.; Klooster, S.; Shapiro, D. J. *J. Biol. Chem.* **1995**, *270*, 1282.
(39) Perez-Martin, J.; Rojo, F.; DeLorenzo, V. *Microbiol. Rev.* **1994**, *58*, 268.
(40) Strauss, J. K.; Roberts, C.; Nelson, M. G.; Switzer, C.; Maher, L. J., III *Proc. Natl. Acad. Sci. U.S.A.*, **1996**, *93*, 9515.

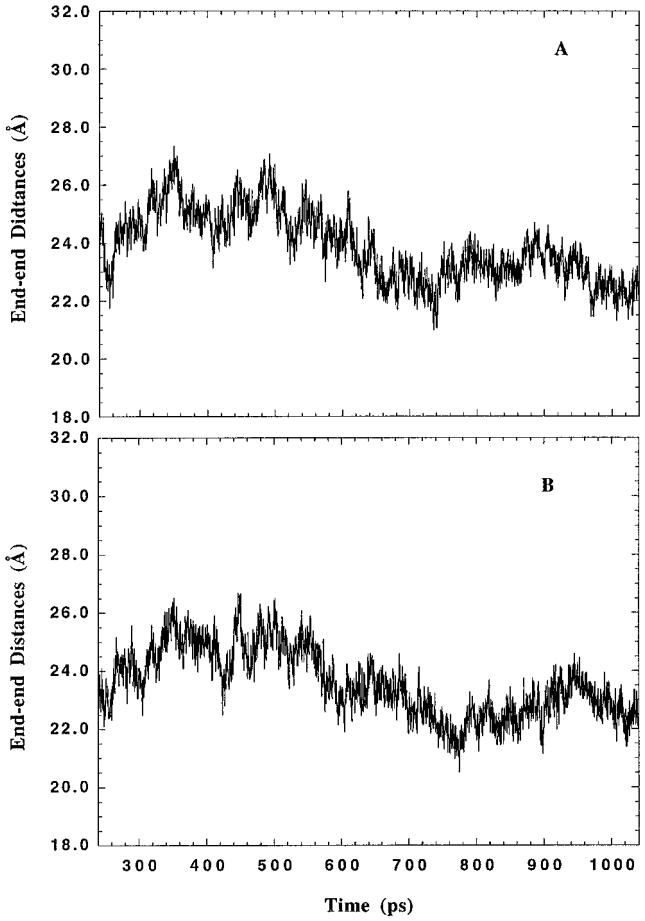

Figure 9. The end-to-end distance histogram for the T (A) and A (B) strands.

full periodic boundary conditions and Na^+ and Cl^- counterions using the Ewald method. Our results show that Watson−Crick hydrogen bonds, without any restraints, remain intact throughout the simulation. Even the two ends were not frayed. The determination of the helical parameters and the sugar pucker pseudorotaton of the average structure from the dynamics run shows that the overall structure is equilibrated at a B-DNA conformation and the RNG strand takes on the general conformation of the DNA backbone. The second base pair next to both 5′ and 3′ ends undergo certain degrees of either unwinding or change of rise in order to provide more space for the bending distortion. Due to the electrostatic attractions between DNA polyanion and RNG polycation, the overall structure of the hybrid complex is more compact than a DNA·RNA complex. The most notable structural features are the minor groove width narrowing (3 Å) compared to the like DNA·RNA hybrid and the overall tract bending. The bending angle measured between the local axis vectors of the first and last helical axis segments is about 33° for the averaged structure. Propeller twist (associated with three-centered hydrogen bonding, helping the stabilization of the hybrid double helix) up to −30°, native to DNA AT base pairing, was also observed. The major groove width does not increase by more than 1 Å, not as much as the minor groove narrowing, due to bending effects that reduce the overall vertical rise of the local helical bases. The narrower minor groove induces a wider major groove and base pair openings (Figure 7C). This provides more accommodating space than in a usual DNA·RNA hybrid for a third strand forming a triplex. Spines of hydration are observed in both minor and major grooves and in both snapshots and the averaged structure. That a portion of the water spines in minor and major grooves have lifetimes equal to or longer than 0.4 ns (the time span for trajectory averaging) is in quantitative agreement with the NMR experimental report that the residence time of the water molecules at their hydration sites ranges from 0.1 to 1 ns[18a,b] for certain DNA oligomers. The sugar pseudorotation phase angles and the ring rotation angles for the DNA strand are within the C3′-endo domain. However, for the RNG strand the pseudorotation angles convert to O4'-endo. Most backbone torsional parameters remained unchanged from the conventional A-DNA/RNA backbone values. Certain RNG backbone torsion angles around the guanidinium group change away from the initially assumed standard A-RNA values to relieve the tensions due to the replacement of the phosphate. However, more importantly, a helical geometry was reestablished with base pair hydrogen bonding to the DNA strand (sequence recognition), after the equilibration.

Acknowledgment. This work was supported by the National Institutes of Health. We express our gratitude to ONR for support of our computer facilities and NIH for the supercomputing hours at Frederick Biomedical Supercomputing Center.

JA970188V